

Direct observation of elastic softening immediately after femtosecond-laser excitation in a phase-change material

Tomoya Kawaguchi ^{1,*} Kazuya Tokuda,¹ Seiya Okada,¹ Makina Yabashi,^{2,3} Tetsu Ichitsubo ^{1,†},
Noboru Yamada,¹ and Eiichiro Matsubara¹

¹*Department of Materials Science and Engineering, Kyoto University, Kyoto 606-8501, Japan*

²*RIKEN SPring-8 Center, Sayo, Japan*

³*Japan Synchrotron Radiation Research Institute, Sayo, Japan*



(Received 25 June 2019; revised manuscript received 6 January 2020; accepted 7 February 2020; published 24 February 2020)

The generation and propagation of photoexcited elastic waves in crystalline $\text{Ge}_2\text{Sb}_2\text{Te}_5$ were analyzed by picosecond time-resolved x-ray diffraction using a femtosecond-laser pump and an x-ray free-electron laser probe technique. The crystalline lattice anisotropically expanded initially in approximately 20 ps after the excitation. This was followed by a periodic oscillation of the lattice strain. The elastic stiffness along the cubic (111) direction had significantly softened during the initial expansion, and the strain magnitude was the largest in the (100) and (110) directions. This indicates that femtosecond-laser excitation creates a shallower interlayer potential between the Te and Ge-Sb layers and eventually leads to softening of the elastic stiffness along the cubic (111) direction. Furthermore, this softened state increases the system's sensitivity to an external stress field. This residual internal stress in a thin film enhances the selective formation of a particular type of variant during the symmetry change from cubic to rhombohedra. This causes the subsequent anisotropic expansion. These phenomena are quite interesting and align with the ultrafast amorphization of this material.

DOI: [10.1103/PhysRevB.101.060302](https://doi.org/10.1103/PhysRevB.101.060302)

The early 1970s featured the demonstration of light-induced rapid crystallization of amorphous semiconductor films. In the beginning of the 1970s, Yamada *et al.* [1] pioneered the development of ultrafast phase-change materials—GeSbTe intermetallic alloys. The pseudobinary system of GeTe-Sb₂Te₃ (GST) thin films, has led to the subsequent development of consumer electronic products such as DVDs and Blu-ray disks, creating a new generation of phase-change optical disks. The reversible phase change between a crystalline and an amorphous phase in this system was achieved through the irradiation of nanosecond laser pulses [2–6]. This was accompanied by a drastic change in their optical reflectivity. This phase-change process generally proceeds via thermal melting. However, reflectivity has also been reported to change at the subpicosecond scale by femtosecond-laser excitation, indicating the possibility of an athermal phase-change process from the crystalline to the amorphous phase [7]. A picosecond-scale amorphization without undergoing a liquid phase has also been suggested via *ab initio* calculation and x-ray absorption spectroscopy [8]. It is essential to understand such an ultrafast phase change to develop faster nonvolatile memory devices. However, there is still an ongoing debate on the mechanisms of the phase change.

Recently, time-resolved x-ray diffraction (TRXRD) with x-ray free-electron laser (XFEL) demonstrated that a clear

image of a rattling motion of the Ge atoms in the Te sublattice was due to femtosecond-laser irradiation in GeTe-based phase-change materials [9]. The rattling motion was associated with loss of resonant bonding [10,11] and ultimately, with amorphization, provided that the fluence of the pump laser was sufficiently large. Similar initial atomic displacements of Ge atoms after femtosecond-laser excitation have also been reported in a single-crystal film using TRXRD [12] and time-resolved electron diffraction [13,14]. Such initial atomic displacement is triggered by a change in the interatomic potential by photoexcitation, which should also reflect the change in elastic properties. Thus, the elastic properties in the transient state following laser excitation are expected to provide insight into the phase-change mechanism triggered by the femtosecond-laser excitation.

Elastic stiffness is usually measured by acoustic and scattering techniques, which use frequency domain. The ultrasonic pulse-echo method [15] and electromagnetic acoustic resonance [16] are typically used to evaluate the elastic constants, in which the resonant frequencies of a shaped sample are measured. On the other hand, the x-ray or neutron inelastic scattering measurements provide a dispersion relation of phonons, with which the elastic constants are also determined in the long-wavelength limit. These frequency-domain approaches are very useful for the evaluation of the static state. However, they are hardly applicable to transient-state measurements such as ultrafast phase changes. Predicting the elastic properties of an excited transient state using *ab initio* calculations, such as density-functional theory, remains an ongoing challenge because of the inherent difficulty in treating the excited state. Time-domain measurement is an alternative

*Present address: Institute for Materials Research, Tohoku University, Sendai 980-8577, Japan; tkawaguchi@imr.tohoku.ac.jp

†Present address: Institute for Materials Research, Tohoku University, Sendai 980-8577, Japan.

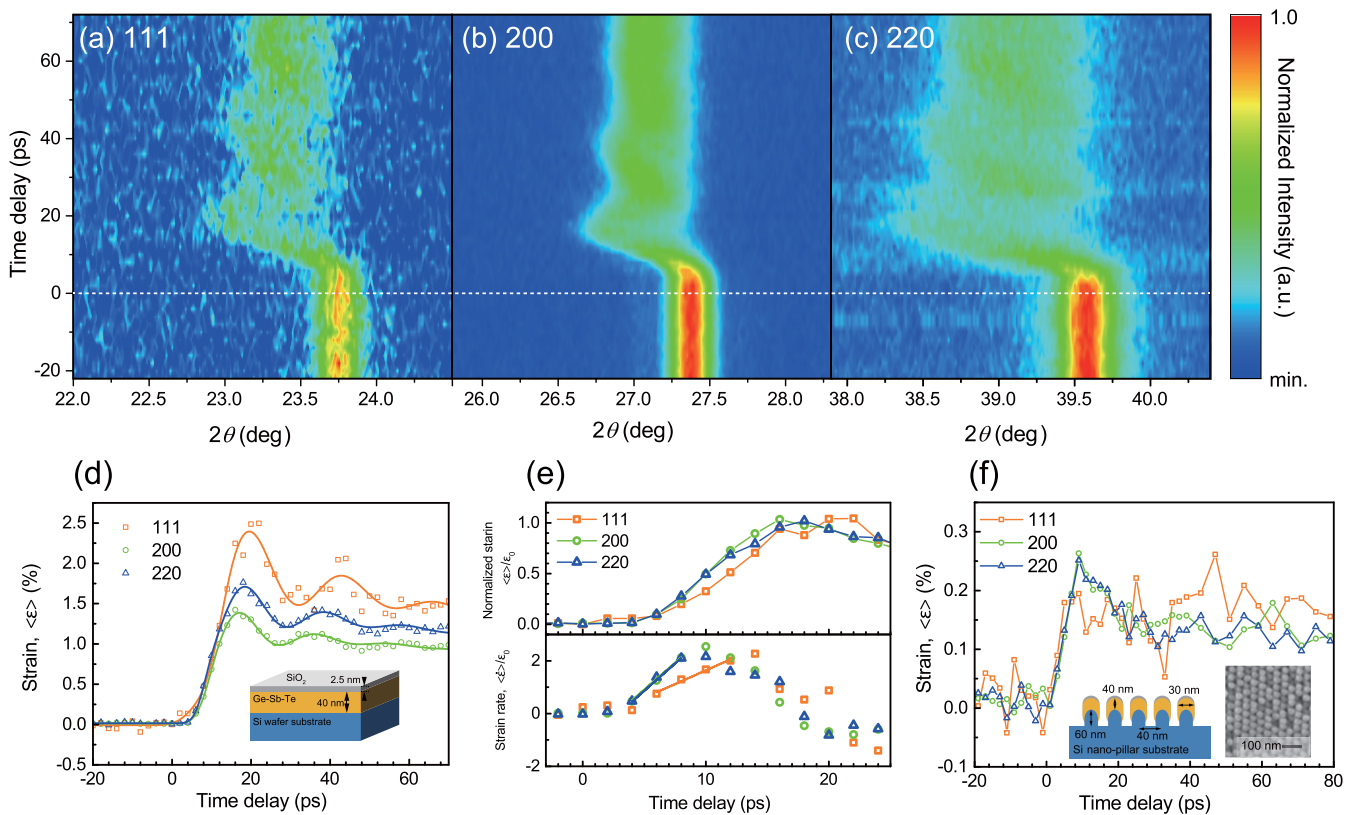


FIG. 1. Time-dependent x-ray powder diffraction patterns for (a) 111, (b) 200, and (c) 220 acquired from the thin-film $\text{Ge}_2\text{Sb}_2\text{Te}_5$ sample after the femtosecond-laser irradiation. (d) Time-dependent strain of the thin-film sample after the femtosecond-laser irradiation. Solid lines indicate the best-fit curves using a step function with oscillation and exponential decays as described in Eq. (1). The inset is a schematic of the thin-film sample. (e) Normalized strain of the thin-film sample at $t = 0$ ps (upper panel) and its first derivative (lower panel). Line segments indicate the time region where the slopes were evaluated. (f) Time-dependent strain of the nanodot sample after the femtosecond-laser irradiation. The insets are a schematic and scanning electron microscopy image of the nanodot sample. In (d), (e), and (f), the orange square, green circle, and blue triangle correspond to the (111), (200), and (220) planes, respectively.

approach for evaluating elastic properties and/or the phonons of the sample. This approach was realized by pump-probe measurements, due to the emergence of an ultrashort pulse x-ray source such as the XFEL. For example, Hayashi *et al.* [17,18] reported that an acoustic pulse echo in a thick film of a single-crystal semiconductor can be probed by TRXRD using triple-crystal diffractometry to evaluate the strain component. Furthermore, Trigo *et al.* [19] reported that the dispersion relation of phonons can be evaluated from the time evolution of the x-ray diffuse scattering after the femtosecond-laser excitation. Thus, the time-domain measurement at the reciprocal point, i.e., Bragg reflection, corresponds to the observation of the phonons in the long-wavelength limit, i.e., the elastic wave. Ultrafast TRXRD is therefore capable of monitoring elastic stiffness of a material under photoexcitation in a certain direction through the selection of the measured diffraction indices [20].

In the present study, we conducted a pump-probe TRXRD measurement in the reversible regime on polycrystalline GST thin films to determine the elastic properties of the material following femtosecond-laser irradiation. An x-ray powder diffraction process enabled the simultaneous acquisition of 111, 200, and 220 diffractions, allowing discussion on the anisotropy of the elastic properties. The observed strain

oscillation was analyzed on the basis of a classical wave-propagation description. The transient lattice deformation associated with a symmetry change from cubic to rhombohedral was also discussed in light of the effect of stress bias on thin films. This was done by comparing with the phase-change material deposited on a nanodot substrate, in which the in-plane stress is relatively low.

The thin-film [Fig. 1(d) inset] and nanodot samples [Fig. 1(f) inset] were prepared by radio frequency magnetron sputtering and subsequent heat treatment (refer to the Supplemental Material [21] for details of sample preparation and measurement). The nanodot sample was prepared to reveal the effect of the sample morphology on the ultrafast lattice deformation in the present study. Note that the nanodot sample itself had been originally developed to increase recording density by suppressing the thermal diffusion and utilizing the plasmonic electric field [22]. The pump-probe TRXRD measurement was performed at the BL3 beamline of SACLA [23] in reflection geometry, in which the lattice spacing change of the material perpendicular to the sample surface was observed by XRD. This is in contrast to our previous study with transmission geometry [9], in which the scattering vector was nearly parallel to the sample surface. The three XRD peaks of 111, 200, and 220 from the thin-film sample

TABLE I. Experimentally determined parameters for the response to the femtosecond-laser excitation in the thin-film sample and the direction dependence of the longitudinal elastic constant. Those under the static state were obtained using XRD and *ab initio* calculations [24]. The crystal density ($\rho = 6300 \text{ kg m}^{-3}$) was used to determine the elastic constants.

State		[111]	[220]	[200]
Photoexcited (oscillation)	ϵ_{exp} (%)	1.02(5)	0.74(11)	0.586(9)
	ϵ_{osc} (%)	0.4(11)	0.27(5)	0.25(5)
	τ_{exp} ($\times 10^2$ ps)	1.8(4)	2.4(2)	2.6(2)
	τ_{osc} (ps)	14(11)	14.2(2)	13.1(2)
	T_{osc} (ps)	24(13)	20.3(5)	19.3(6)
	$C_{[hkl]}$ (GPa)	31(4)	43(2)	48(3)
Photoexcited (initial expansion)	$C_{[hkl]}/C_{[200]}$	0.65(8)	0.90(7)	1
	$C_{[hkl]}/C_{[200]}$	0.50(4)	0.98(7)	1
Static [24] (experimental)	$C_{[hkl]}$ (GPa)	29(4)	32(4)	41(6)
	$C_{[hkl]}/C_{[200]}$	0.7(13)	0.8(14)	1
Static [24] (calculation)	$C_{[hkl]}$ (GPa)	41(3)	45(3)	58(4)
	$C_{[hkl]}/C_{[200]}$	0.70(7)	0.78(7)	1

initially shifted to a lower angle, accompanied by a decrease in peak intensities immediately after the laser excitation until ~ 18 ps. Subsequently, the peaks showed an oscillation in the scattering angles [Figs. 1(a)–1(c)]. This intensity drop immediately after the near-infrared (NIR)–laser excitation reflects the displacement of the atomic position from the static state. We had previously found that the off-centered rattling motion of the Ge and Sb atoms in the Te sublattice and its accompanying increase in the Debye-Waller factor consistently explained the orientational dependence of the observed intensity changes in terms of change in the structure factor of this material [9]. As such, this study focused on the drastic peak shifts from ~ 4 to 18 ps and the subsequent oscillations that were observed.

The strains along the $\langle 111 \rangle$, $\langle 200 \rangle$, and $\langle 220 \rangle$ directions were evaluated by comparing the lattice spacing with and without the NIR-laser excitation for both the thin-film and the nanodot sample [Figs. 1(d)–1(f)]. Distinct oscillations were observed in every direction for the thin-film sample, whereas such oscillations were hardly observed in the nanodot sample at the present signal-to-noise ratio [Fig. 1(f)]. The oscillation observed in the thin-film sample involves the initial expansion induced by the femtosecond-laser stimulation (ϵ_{exp}), inertia term (i.e., the strain amplitude) of the oscillation (ϵ_{osc}), two relaxation times for the oscillation (τ_{osc}), thermal dissipation (τ_{exp}), and period of the oscillation (T_{osc}). Thus, we fit Eq. (1) to the photoinduced strain data (Table I):

$$\epsilon = \left\{ \epsilon_{\text{exp}} \exp\left(-\frac{t}{\tau_{\text{exp}}}\right) + \epsilon_{\text{osc}} \sin[2\pi(t + t_0)/T_{\text{osc}}] \times \exp\left(-\frac{t}{\tau_{\text{osc}}}\right) \right\} \theta(t), \quad (1)$$

where t is the time and $\theta(t)$ is a smooth step function described as $\text{erf}(\omega_{\text{exp}}t) + 1$.

The oscillation period of the 200 diffraction in the thin-film sample was evaluated to 19.3(6) ps. This is in good agreement with $L/v_L = 16$ ps, where L is the thickness of the thin-film sample, i.e., 40 nm, and v_L is the longitudinal sound velocity along the $[200]$ direction, i.e., 2551 m s^{-1} , calculated from an elastic constant of 41 GPa [24] and a density of 6300 kg m^{-3} . The numerical simulation using the classical wave equation also reproduced the experimentally observed strain oscillation qualitatively [21]. Thus, there is evidence that this observed oscillation corresponds to the elastic wave propagating in the thin film along the thickness direction. Notably, a longitudinal wave was predominantly observed in the present XRD because the scattering vector was perpendicular to the sample surface. In contrast, distinct oscillations were barely visible in the nanodot sample at the present signal-to-noise ratio [Fig. 1(f)]. The lattice expansion following photoexcitation indicates that the photoexcitation also yields an accompanying elastic wave in the nanodot sample. However, the elastic waves are considered to have been generated at the top of the pillar and from the side surface of the pillar, eventually scattering in the relatively complicated morphology of the nanodot. This yielded the damped strain oscillation when XRD observes the averaged strain in the material. The speed of the initial expansion in the thin-film sample depended on the crystalline orientation [Fig. 1(e)]; the lattice expansion of $[111]$ was slower than those of the other directions. Notably, the expansion magnitudes of the thin-film sample were also dependent on the crystalline orientation. This anisotropic expansion indicates the symmetry change from the cubic to the rhombohedral structure by laser excitation. Such anisotropic expansion was not observed in the nanodot sample [Fig. 2(f)].

The dynamics of the photoinduced strain in the thin-film sample were further modeled by one-dimensional wave propagation along the thickness direction with a fixed end at one end to evaluate stiffness under photoexcitation [21]. Based on the solution of the wave equation in the present condition, the velocity of the initial expansion was related to the elastic constants from Supplemental Material Eq. S2 [21] as follows:

$$\langle \dot{\epsilon} \rangle / \langle \epsilon_0 \rangle = \frac{\gamma C_{[hkl]}}{\rho} \tau, \quad (2)$$

where $\langle \dot{\epsilon} \rangle$ is the derivative of $\langle \epsilon \rangle$, i.e., $d\langle \epsilon \rangle / dt$; $\langle \epsilon \rangle$ is the averaged strain over the whole depth of the thin-film sample observed by XRD; $\langle \epsilon_0 \rangle$ is the averaged strain in the initial state; $C_{[hkl]}$ is the longitudinal elastic constant of the $[hkl]$ direction; τ is the time immediately after the lattice expansion; and γ is the constant coefficient independent of $C_{[hkl]}$ and τ . The elastic constants were also calculated from the substantially observed oscillation period, T , in the strain observed in TRXRD as

$$C_{[hkl]} = \frac{\rho}{T^2} \left(\frac{4L}{2n-1} \right)^2. \quad (3)$$

Thus, stiffness was evaluated at two time regions, i.e., the initial expansion and the subsequent strain oscillation, and its time evolution following femtosecond-laser excitation was discussed. For the initial expansion, we evaluated $C_{[hkl]}$ immediately after the femtosecond-laser excitation from the slope of the normalized initial strain rate as described in Eq. (2).

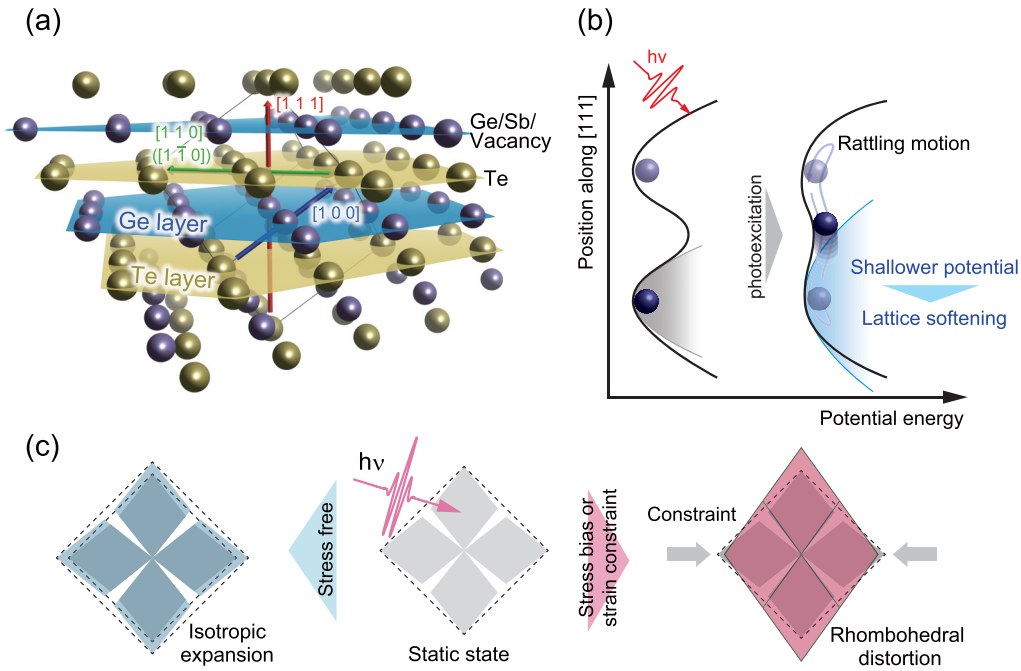


FIG. 2. (a) Structure of rocksalt $\text{Ge}_2\text{Sb}_2\text{Te}_5$. The yellow and purple balls correspond to Te and a mixture of Ge, Sb, and vacancies, respectively. The blue, green, and red arrows indicate the $[100]$ and $[110]$ ($[1\bar{1}0]$) and $[111]$ directions, respectively. (b) Schematics of the interatomic potential before (left) and after (right) the femtosecond-laser excitation. (c) Two different response modes to the femtosecond-laser excitation in the phase-change material. The stress bias or strain constraint within the plane of the thin film forces the excited material to form a single variant structure (right pink rhombus), whereas the lattice expands isotropically without any stress bias (left blue square).

On the other hand, we evaluated the stiffness in the following time region from the substantially observed T using Eq. (3), in which n values need to be determined by comparing the oscillation period experimentally obtained with that estimated from similar compounds.

The T value for the $\langle 111 \rangle$ direction was 24 ps (Table I), whereas the $C_{[111]}$ value of 29 GPa measured under a static condition [24] yielded T values of 75, 25, and 15 ps for the first, second, and third harmonics, respectively. Thus, the predominant oscillation observed in the present measurement was the second harmonics, and $n = 2$ was used in Eq. (3) for the calculations of the other directions. The fundamental wave, $n = 1$, and the higher harmonics, $n \geq 3$, were barely observed because the period (72 ps) was much longer than the decay time of the oscillation (14 ps) and because of the small contributions from the higher harmonics, respectively. The elastic constants at each orientation were calculated from the oscillation periods determined by fitting the data, the sample density of 6300 kg m^{-3} , and the sample thickness of 40 nm, where the SiO_2 cover layer was ignored in the calculation because it was much thinner and lighter than the GST film. Notably, the wave-propagation simulation based on the determined elastic constants was consistent with the experimental observation of the oscillation periods, which validates the present discussion and the analyses [21]. Since the grain size of GST in the film sample was evaluated to be ~ 30 nm from XRD while the thickness of the deposited film was 40 nm, there should be a 10-nm-thick “interface layer” of the polycrystalline GST in all orientations observed in the present study. The sound velocity of the interface layer would affect the observed oscillation period and the corresponding

elastic constants due to its different stiffness. Nevertheless, the determined elastic constants for each orientation in this study ranged between those obtained from XRD and *ab initio* calculation of the static state (Table I) [24]. The ratio of the elastic constants, $C_{[hkl]}/C_{[200]}$, was also calculated to compare the direction dependence of the stiffness (Table I, oscillation). The ratio along the $[111]$ and $[110]$ directions was slightly smaller and larger than those of the reported values (Table I, static), respectively, indicating a slight softening along the $[111]$ direction by photoexcitation. Note that the ratios of the elastic constants are their upper limits as ratios are always overestimated due to the interface layer with the different stiffness [21]. Interestingly, the elastic constants at each direction observed under the photoexcitation apparently did not hold the relation under the cubic symmetry: $C_{[111]} = (4C_{[110]} - C_{[100]})/3$. The $C_{[111]}$ of 31 GPa observed in this study was much smaller than that estimated from the other directions under the cubic symmetry, i.e., 41.3 GPa. This indicates the significant softening along the $[111]$ direction and symmetry change as the precursor phenomena of the phase change. The tendency along the $[111]$ direction softening was more significant immediately after photoexcitation, as per the expansion speed with Eq. (2). The ratio along the $[111]$ direction significantly decreased and that along the $[110]$ direction slightly increased to that of $[100]$ (Table I, initial expansion). This indicates that the relative softening along the $[111]$ direction was due to the laser excitation compared to that along the other directions.

The crystal structure of GST is a cubic rocksalt structure and is also understood as a layered structure of Te and Ge layers. The Ge layers consist of Sb and vacancy in addition to

Ge, along the [111] direction [Fig. 2(a)]. The [111] and [100] directions are exactly and partially along the stacking direction of the layer structure, respectively. These elastic properties would therefore be more sensitive to the interatomic potential between Te and Ge/Sb than the other direction. In contrast, the [100] direction is an in-layer direction, reflecting the potential between the same or similar elements, i.e., Te-Te and Ge/Sb/vacancy-Ge/Sb/vacancy. Thus, the significant softening along the [111] direction after laser excitation can be attributed to the change in the interatomic potential between Ge(Sb) and Te because the stiffness reflects on the curvature of the potential.

In the static state, Ge(Sb) atoms form six bonds with Te to produce the Ge(Sb)Te₆ octahedron in the rocksalt structure. The electron deficiency of Ge required to form the complete six covalent bonds yields two types of bonds: three strong bonds and three weak bonds. Consequently, Ge atoms are slightly displaced toward one of the eight equivalent $\langle 111 \rangle$ directions from the center of the octahedron. In contrast to GeTe in which the Ge-displacement direction is ordered in a crystal, Ge atoms in GST randomly occupy one of the eight equivalent stable sites, and eventually are slightly off-centered in the octahedron [25,26]. It has been reported that femtosecond-laser excitation induces a significant displacement of Ge from the stable site and, eventually, a rattling motion when the Debye-Waller factor is increased [Fig. 2(b)] [9]. This observation also implies that femtosecond-laser excitation makes the interatomic potential shallower to ease the atomic motion on the bottom of the potential. Such potential change is also expected to decrease the curvature of the bottom of the potential, which is the stiffness along the [111] direction. Thus, the present result is consistent with the previously reported results of rattling motion and provides a macroscopic aspect of the initial atomic motion induced by the femtosecond-laser excitation. Based on the oscillation analysis of the stimulated strain, this softening immediately relaxes after the initial expansion within ~ 15 ps by transferring the energy from the electron system to the lattice system.

The anisotropic expansion experimentally observed in the thin-film sample [Fig. 1(d)] suggests that one type of $\langle 111 \rangle$ variant dominates the others. However, it is naturally expected that eight equivalent $\langle 111 \rangle$ directions in a rocksalt GST (variants) may equivalently expand in a photoexcited GST lattice and eventually keep the cubic symmetry as seen in the nanodot sample [Fig. 1(f)]. The XRD with a change in the angle, χ , between the scattering vector and the surface normal of the thin-film sample indicates that the thin-film sample has in-plane tensile strain within the film [21]. Furthermore, similar anisotropic expansion was observed as the thermal strain in the thin-film sample at the elevated temperature. Here, the mismatch of the thermal expansion coefficients of a Si substrate and GST caused biaxial compressive stress. Thus, the present symmetry change from cubic to rhombohedral is understood to be from the strain/stress bias as seen in

other systems [Fig. 2(c)]. The phase transformation proceeds so that the system appropriately adjusts to the external field [27,28]. The present anisotropic expansion itself is not a peculiar characteristic of the laser excitation. However, the magnitude of the anisotropy was significantly enhanced by the femtosecond-laser excitation so that the thermal expansion is hardly achieved, which could be a precursory phenomenon of the ultrafast phase change in this material.

In summary, the transient change in the elastic stiffness of a crystalline GST film immediately after femtosecond-laser excitation was measured by TRXRD with an XFEL. Anisotropic expansion followed by strain oscillation was observed in cubic 111, 200, and 220 diffractions of the thin-film sample. The elastic constants determined from the oscillation period were in good agreement with those measured under the static state. The orientation dependence of the initial expansion velocity indicates a significant softening along the [111] direction immediately after the femtosecond-laser excitation, i.e., $t < \sim 15$ ps. This could be attributed to the nonthermal interatomic potential change triggered by the femtosecond-laser excitation, eventually leading to the reported initial displacement and rattling motion of the Ge atoms. This softening rapidly relaxed during the period of the first elastic wave propagation, and it lingered in the subsequent oscillation with a smaller magnitude. On the other hand, the anisotropic expansion indicates the symmetry change from cubic to rhombohedral, whereas the isotropic expansion was expected because of the cubic symmetry. The strain/stress bias due to the constraint from the substrate enhances the growth of a certain variant of the rhombohedral crystal that most efficiently relaxes the strain in the excited state. This significant softening could be the initial stage of the ultrafast structural change from the crystalline to the amorphous phase. Subsequent variant-selected rhombohedral deformation could affect the resultant phase-change behavior. The present time-domain measurement enables monitoring the transient state of the elastic properties, which can also be used as a powerful tool for understanding other ultrafast phase transformations.

We would like to thank Professor Y. Tanaka and all the beamline scientists, namely, Dr. K. Ogawa and Dr. S. Owada at SACLA, for maintaining the high performance of the XFEL throughout our experiments. We are deeply indebted to Dr. R. Kojima, K. Kawahara, A. Tsuchino, and Dr. K. Nishiuchi (Panasonic) for their helpful assistance in the sample preparations. We also thank Professor Hiroshi Tanimura at Tohoku University for the fruitful discussion. The experiments were performed at the BL3 beamline of SACLA, with the approval of the Japan Synchrotron Radiation Research Institute (JASRI) (Proposals No. 2012B8044, No. 2013A8048, No. 2013B8053, No. 2014A8037, and No. 2014B8062). This work was supported by the X-ray Free Electron Laser Priority Strategy Program (MEXT). The crystalline-structure models were drawn using the VESTA3 software [29].

[1] N. Yamada, E. Ohno, N. Akahira, K. Nishiuchi, K. Nagata, and M. Takao, *Jpn. J. Appl. Phys.* **26**, 61 (1987).

[2] M. Wuttig and N. Yamada, *Nat. Mater.* **6**, 824 (2007).

[3] T. Matsunaga, J. Akola, S. Kohara, T. Honma, K. Kobayashi, E. Ikenaga, R. O. Jones, N. Yamada, M. Takata, and R. Kojima, *Nat. Mater.* **10**, 129 (2011).

- [4] M. Chen, K. A. Rubin, and R. W. Barton, *Appl. Phys. Lett.* **49**, 502 (1986).
- [5] N. Yamada, E. Ohno, K. Nishiuchi, N. Akahira, and M. Takao, *J. Appl. Phys.* **69**, 2849 (1991).
- [6] N. Yamada, *Phys. Status Solidi* **249**, 1837 (2012).
- [7] M. Konishi, H. Santo, Y. Hongo, K. Tajima, M. Hosoi, and T. Saiki, *Appl. Opt.* **49**, 3470 (2010).
- [8] A. Kolobov, P. Fons, M. Krbal, and J. Tominaga, *J. Non.-Cryst. Solids* **358**, 2398 (2012).
- [9] E. Matsubara, S. Okada, T. Ichitsubo, T. Kawaguchi, A. Hirata, P. F. Guan, K. Tokuda, K. Tanimura, T. Matsunaga, M. W. Chen, and N. Yamada, *Phys. Rev. Lett.* **117**, 135501 (2016).
- [10] G. Lucovsky and R. M. White, *Phys. Rev. B* **8**, 660 (1973).
- [11] K. Shportko, S. Kremers, M. Woda, D. Lencer, J. Robertson, and M. Wuttig, *Nat. Mater.* **7**, 653 (2008).
- [12] K. V. Mitrofanov, P. Fons, K. Makino, R. Terashima, T. Shimada, A. V. Kolobov, J. Tominaga, V. Bragaglia, A. Giussani, R. Calarco, H. Riechert, T. Sato, T. Katayama, K. Ogawa, T. Togashi, M. Yabashi, S. Wall, D. Brewster, and M. Hase, *Sci. Rep.* **6**, 20633 (2016).
- [13] M. Hada, W. Oba, M. Kuwahara, I. Katayama, T. Saiki, J. Takeda, and K. G. Nakamura, *Sci. Rep.* **5**, 13530 (2015).
- [14] J. Hu, G. M. Vanacore, Z. Yang, X. Miao, and A. H. Zewail, *ACS Nano* **9**, 6728 (2015).
- [15] H. B. Huntington, *Phys. Rev.* **72**, 321 (1947).
- [16] M. Hirao and H. Ogi, *Ultrasonics* **35**, 413 (1997).
- [17] Y. Hayashi, N. Tsukuda, E. Kuramoto, Y. Tanaka, and T. Ishikawa, *J. Synchrotron Radiat.* **12**, 685 (2005).
- [18] Y. Hayashi, Y. Tanaka, T. Kirimura, N. Tsukuda, E. Kuramoto, and T. Ishikawa, *Phys. Rev. Lett.* **96**, 115505 (2006).
- [19] M. Trigo, M. Fuchs, J. Chen, M. P. Jiang, M. Cammarata, S. Fahy, D. M. Fritz, K. Gaffney, S. Ghimire, A. Higginbotham, S. L. Johnson, M. E. Kozina, J. Larsson, H. Lemke, A. M. Lindenberg, G. Ndabashimiye, F. Quirin, K. Sokolowski-Tinten, C. Uher, G. Wang, J. S. Wark, D. Zhu, and D. A. Reis, *Nat. Phys.* **9**, 790 (2013).
- [20] E. Matsubara and T. Ichitsubo, *SPRING-8/SACLA Res. Rep.* **7**, 100 (2019).
- [21] See Supplemental Material at <http://link.aps.org/supplemental/10.1103/PhysRevB.101.060302> for experimental and data analysis details, and numerical simulation.
- [22] N. Yamada, R. Kojima, K. Hisada, T. Mihara, A. Tsuchino, N. Fujinoki, M. Birukawa, T. Matsunaga, N. Yasuda, Y. Fukuyama, K. Ito, Y. Tanaka, S. Kimura, and M. Takata, *Adv. Opt. Mater.* **1**, 820 (2013).
- [23] H. Tanaka and M. Yabashi *et al.*, *Nat. Photon.* **6**, 540 (2012).
- [24] R. Cecchini, K. Kohary, A. Fernández, M. Cabibbo, and A. Marmier, *J. Phys. Chem. C* **120**, 5624 (2016).
- [25] A. V. Kolobov, P. Fons, A. I. Frenkel, A. L. Ankudinov, J. Tominaga, and T. Uruga, *Nat. Mater.* **3**, 703 (2004).
- [26] M. Krbal, A. Kolobov, P. Fons, R. E. Simpson, T. Matsunaga, J. Tominaga, and N. Yamada, *Phys. Rev. B* **84**, 104106 (2011).
- [27] T. Ichitsubo, K. Tanaka, M. Koiwa, and Y. Yamazaki, *Phys. Rev. B* **62**, 5435 (2000).
- [28] T. Ichitsubo, M. Nakamoto, K. Tanaka, and M. Koiwa, *Mater. Trans. JIM* **39**, 24 (1998).
- [29] K. Momma and F. Izumi, *J. Appl. Crystallogr.* **44**, 1272 (2011).